

ARE ULTRA-LONG GAMMA-RAY BURSTS CAUSED BY BLUE SUPERGIANT COLLAPSARS, NEWBORN MAGNETARS, OR WHITE DWARF TIDAL DISRUPTION EVENTS?

KUNIHITO IOKA^{1,2,3}, KENTA HOTOKEZAKA⁴, AND TSVI PIRAN⁴

ABSTRACT

Ultra-long gamma-ray bursts (*u*GRBs) are a new population of GRBs with extreme durations of $\sim 10^4$ s. Leading candidates for their origin are blue supergiant collapsars, magnetars, and white dwarf tidal disruption events (WD-TDEs) caused by massive black holes (BHs). Recent observations of supernova-like (SN-like) bumps associated with *u*GRBs challenged both the WD-TDE and the blue supergiant models because of the detection of SNe and the absence of hydrogen lines, respectively. We propose that WD-TDEs can accommodate the observed SN-like bumps if the fallback WD matter releases energy into the unbound WD ejecta. The observed ejecta energy, luminosity, and velocity are explained by the gravitational energy, Eddington luminosity, and escape velocity of the formed accretion disk, respectively. We also show that the observed X-rays can ionize the ejecta, eliminating lines. The SN-like light curves (SN 2011kl) for the *u*GRB 111209A are consistent with all three models, although a magnetar model is unnatural because the spin-down time required to power the SN-like bump is a hundred times longer than the GRB. Our results imply that TDEs are a possible energy source for SN-like events in general and for *u*GRBs in particular.

Subject headings: black hole physics — galaxy: nuclei — gamma-ray burst: general — gamma-ray burst: individual (GRB 111209A) — stars: black holes — stars: magnetars — stars: massive — supernovae: general

1. INTRODUCTION

A rich diversity of gamma-ray burst (GRB) phenomena has been recognized over the last decade. Long GRBs are thought to arise from collapsars, i.e., the collapse of massive stars (Paczynski 1998) associated with jets penetrating the stellar envelope (MacFadyen & Woosley 1999). Short GRBs (sGRBs) are most likely caused by mergers of neutron stars (Eichler et al. 1989). Flares of soft gamma-ray repeaters most likely result from the sudden release of energy via magnetic field reconnection (e.g., Thompson & Duncan 1993, 1995; Ioka 2001). Low-luminosity GRBs are still mysterious but could be produced by shock or jet breakouts from stellar envelopes or winds (Kulkarni et al. 1998; Toma et al. 2007; Waxman et al. 2007; Bromberg et al. 2011a; Nakar 2015; Irwin & Chevalier 2016). Besides GRBs, an unusual class of objects similar to Swift J1644+57 (GRB 110328A) (Bloom et al. 2011; Burrows et al. 2011; Levan et al. 2011; Zauderer et al. 2011) is considered to be tidal disruption events (TDEs) that launch relativistic jets (Bloom et al. 2011; Krolik & Piran 2011).

Recently a new class of GRBs has been identified—ultra-long GRBs (*u*GRBs) (Gendre et al. 2013; Levan et al. 2014). These include GRB 101225A (the so-called Christmas burst; Campana et al. 2011; Thöne et al. 2011), GRB 111209A, GRB 121027A, GRB 130925A (e.g., Bellm et al. 2014; Evans et al.

2014; Piro et al. 2014), and possibly GRB 141121A (Cucchiara et al. 2015), which are listed in Table 1. Additional *u*GRB candidates were recently reported by Lien et al. (2016). The duration of these *u*GRBs, $\sim 10^4$ s, is much longer than that of the conventional long GRBs, while the isotropic energy is comparable. Since the event rate is also comparable, $\sim 1 \text{ Gpc}^{-3} \text{ yr}^{-1}$ (Levan et al. 2014), these *u*GRBs are not negligible from the point of view of the total energy budget compared with the long GRBs, possibly manifesting themselves in the neutrino sky (Murase & Ioka 2013). But it is still unclear whether these bursts are simply extreme examples of the long GRB class (Zhang et al. 2014) or not (Boer et al. 2015; Gao & Mészáros 2015).

Several models have been proposed for the *u*GRBs. Three representative models are blue supergiant collapsar (Kashiyama et al. 2013; Nakauchi et al. 2013), newborn magnetar (Greiner et al. 2015, hereafter G15), and white dwarf TDE (WD-TDE) models (Gendre et al. 2013; Levan et al. 2014; MacLeod et al. 2014)⁵. The blue supergiant model is a simple extension of the collapsar model for long GRBs, in which the ultra-long duration arises due to the much more extended envelope of the progenitor star, which leads to a much longer activity of the central engine as discussed in the context of Population III GRBs (Suwa & Ioka 2011; Nagakura et al. 2012). In the magnetar model, a rotating neutron star launches a magnetized jet for the duration of its spin-down time (Usov 1992; Thompson & Duncan 1993; Wheeler et al. 2000; Thompson et al. 2004). The WD-TDE model is also a natural extension of a model for Swift J1644+57 to slightly shorter duration. This is consistent with the orbital time of the most bound debris (Rees 1988) and with the variability on a scale of a few hundred seconds

kunihito.ioka@yukawa.kyoto-u.ac.jp

¹ Center for Gravitational Physics, Yukawa Institute for Theoretical Physics, Kyoto University, Kyoto 606-8502, Japan

² Theory Center, Institute of Particle and Nuclear Studies, KEK, Tsukuba 305-0801, Japan

³ Department of Particle and Nuclear Physics, SOKENDAI (The Graduate University for Advanced Studies), Tsukuba 305-0801, Japan

⁴ Racah Institute of Physics, The Hebrew University of Jerusalem, Jerusalem 91904, Israel

⁵ See Gao et al. (2016) and Perets et al. (2016) for other models.

TABLE 1
*ul*GRBs

GRB	z	T_{90} (s)	E_{iso} (erg)	Late Decay	Light Radii of Hosts (pc)	GRB Position (pc)
GRB 101225A	0.85	> 7000	1.2×10^{52}	...	< 600 (80% LR)	< 150
GRB 111209A	0.67	> 10000	5.2×10^{52}	$t^{-1.36 \pm 0.05}$	700 (80% LR)	< 250
GRB 121027A	1.77	> 6000	7×10^{52}	$t^{-1.44 \pm 0.08}$
GRB 130925A	0.35	~ 4500	1.5×10^{53}	$t^{-1.32}$ ($t > 300$ ks)	2400 (50% LR)	< 600
GRB 141121A	1.469	~ 1410	8×10^{52}	$t^{-2.14 \pm 0.34}$ ($t > 5$ days)

NOTE. — Data from Levan et al. (2014); Horesh et al. (2015); Piro et al. (2014); Cucchiara et al. (2015); Schady et al. (2015).

during the burst (Krolik & Piran 2011) if the disrupted star is a WD.

The blue supergiant collapsar and the WD-TDE models have been challenged recently by the observations of supernova-like (SN-like) bumps associated with *ul*GRBs. Levan et al. (2014) have noticed SN-like bumps in infrared/optical afterglows ~ 10 days after some *ul*GRBs. The luminosities of these SN-like bumps are between those of SNe Ic associated with long GRBs and superluminous supernovae (SLSNe) (e.g., Gal-Yam 2012), and they are similar to rapidly rising gap transients (Arcavi et al. 2016). Nakauchi et al. (2013) interpreted the SN-like bump within the blue supergiant model as emission from an expanding cocoon, which is energized by a jet during its propagation through the progenitor star. However, G15 have reported detailed light curves and spectra of SN 2011kl associated with the *ul*GRB 111209A. They discarded both the blue supergiant model and the WD-TDE model because of the absence of hydrogen lines and the detection of the SN, respectively. By elimination, they are led to develop a magnetar model by modifying that of Kasen & Bildsten (2010) for SLSNe.

We re-examine here the origin of the SN-like bumps associated with *ul*GRBs, concluding that the current observations cannot exclude either WD-TDE or blue supergiants as the progenitors of *ul*GRBs. We suggest that WD-TDEs can produce an SN-like bump if the fallback WD matter releases its gravitational energy into the surrounding tidally unbound WD ejecta. As far as the lack of hydrogen lines is concerned, we note that the observed X-ray emission that arises from the central engine could ionize the ejecta, removing hydrogen lines as well as carbon and oxygen lines from the spectrum of SN-like bumps.

After submitting our paper, we noticed Leloudas et al. (2016), discussing that the SLSN-like transient ASASSN-15lh could originate from a TDE from a Kerr black hole (BH). This may be a normal-star TDE but an analogue of our case. Observationally, many optical TDEs are discovered by exploring the gap between SNe and SLSNe (e.g., Arcavi et al. 2014). Thus some SN/SLSN-like events would be caused by TDEs.

The organization of this paper is as follows. In Section 2, we examine the bolometric light curve of the SN-like bump observed in the *ul*GRB 111209A in order to discriminate whether the energy injection is explosive or continuous before going into specific models. In Section 3, we reproduce the multi-band light curves of each model and discuss the implications of the parameters obtained. We find that the model parameters are somewhat

unnatural for a magnetar model. In Section 4, we show that the observed X-ray emission could ionize the ejecta, erasing lines in the spectrum. In Section 5, we calculate the probability for the location of *ul*GRBs to be concentrated in the nuclei of host galaxies. Section 6 is devoted to the summary and discussions.

We adopt a redshift $z = 0.677$ with a luminosity distance $d = 4080$ Mpc for GRB 111209A (Levan et al. 2014), and a standard Λ CDM cosmology with $\Omega_\Lambda = 0.73$, $\Omega_m = 0.27$ and $H_0 = 71$ km s $^{-1}$ Mpc $^{-1}$.

2. THE BOLOMETRIC LIGHT CURVE OF THE SUPERNOVA-LIKE BUMP

We begin, in Sec. 2.1, with a discussion of the global characteristics of ejecta that can produce an SN-like bump. We obtain an order of magnitude estimate of physical quantities. We then examine, in Sec. 2.2, the light curve of the SN-like bump SN 2011kl associated with *ul*GRB 111209A. Our goal is to determine whether the energy injection is explosive (with a short timescale compared to the bump) or continuous (with a timescale comparable to the bump), before discussing specific models in Sec. 3.

2.1. Global characteristics of the ejecta

The observations at the peak of the SN-like bump can constrain the physical properties of the ejecta. The peak time of the bump, $t_p \sim 10$ days, is much longer than the *ul*GRB 111209A. It can be identified as the diffusion timescale of photons in the ejecta:

$$t_d = \sqrt{\frac{3\kappa M}{4\pi v c}} \sim 15 \text{ day} \left(\frac{\kappa}{0.1 \text{ cm}^2 \text{ g}^{-1}} \right)^{1/2} \left(\frac{M}{1 M_\odot} \right)^{1/2} \left(\frac{v}{10^9 \text{ cm s}^{-1}} \right)^{-1/2} (1)$$

where M , κ , and v ($\ll c$, the speed of light) are the mass, opacity, and velocity of the ejecta (Arnett 1979, 1980; Dexter & Kasen 2013). The photospheric velocity is estimated from the peak temperature T and luminosity L as

$$v \sim \sqrt{\frac{L}{4\pi t_p^2 \sigma T^4}} \sim 2 \times 10^9 \text{ cm s}^{-1} \left(\frac{T}{10^4 \text{ K}} \right)^{-2}, \quad (2)$$

where $L \sim 3 \times 10^{43}$ erg s $^{-1}$ is the observed bolometric luminosity (G15) and σ is the Stefan–Boltzmann constant. The spectrum observed by X-shooter shows a rest-frame peak at 3000 Å (G15), implying a blackbody temper-

ature of $\sim 10^4$ K or higher.⁶ On the other hand, the kinetic energy,

$$E_k = \frac{1}{2} M v^2 \sim 1 \times 10^{51} \text{ erg} \left(\frac{M}{1 M_\odot} \right) \left(\frac{v}{10^9 \text{ cm s}^{-1}} \right)^2 \quad (3)$$

should be larger than the total radiated energy $\sim L t_p \sim 3 \times 10^{49}$ erg since the radiation pressure accelerates the ejecta during the optically thick regime. Thus the mass and velocity of the ejecta are narrowed down to $0.3 \lesssim M \lesssim 3 M_\odot$ and $3 \times 10^8 \lesssim v \lesssim 2 \times 10^9 \text{ cm s}^{-1}$, respectively.⁷

2.2. Energy injection: explosive vs. continuous

A crucial question is whether the energy injection into the ejecta is explosive (with a shorter timescale than the peak time) or continuous (with a timescale comparable to the peak time). The blue supergiant model is an example of explosive injection, while continuous injection models include the magnetar and WD-TDE models (see Sec. 3 for details).

The difference in the energy injection history shows up in the light curve of the SN-like bump. The light curve is obtained by the diffusion equation. With a one-zone approximation, this equation is

$$\frac{L(t)}{4\pi R^2} \approx \frac{c}{3\kappa\rho} \frac{E_{\text{int}}/V}{R}, \quad (4)$$

where R , $V = 4\pi R^3/3$, and $\rho = M/V$ are the radius, volume, and density of the ejecta (Arnett 1979, 1980; Dexter & Kasen 2013). The internal energy of the ejecta E_{int} depends on adiabatic losses due to the expansion, an energy injection (with a rate $H(t)$), and emission (with a luminosity $L(t)$):

$$\frac{dE_{\text{int}}}{dt} = -\frac{E_{\text{int}}}{t} + H(t) - L(t), \quad (5)$$

where we assume that the pressure is radiation-dominated. The corresponding luminosity is

$$L(t) = \frac{t_i}{t_d} \frac{E_i}{t_d} e^{-t^2/2t_d^2} + \frac{e^{-t^2/2t_d^2}}{t_d^2} \int_0^t dt' t' e^{t'^2/2t_d^2} H(t'), \quad (6)$$

where E_i is an initial internal energy injected at time t_i into an extended ejecta with a radius vt_i . An SN-like bump can be produced by either the first term, the explosive energy injection, or the second term, the continuous energy injection.

A wide class of profiles of continuous energy injection can be expressed by

$$H(t) = \frac{E}{t_e} \frac{\ell - 1}{(1 + t/t_e)^\ell}, \quad (7)$$

⁶ Shorter wavelengths than the peak are absorbed by metal lines, so that the thermal peak may be bluer than the observed one. G15 also estimate that the photospheric velocity is larger than $2 \times 10^4 \text{ km s}^{-1}$ by using the width of the absorption line, although the lines are useless if the elements are ionized as discussed in Section 4.

⁷ The ejecta mass may be much smaller than the above estimate if we only require that the ejecta reprocesses injected radiation into a lower frequency (Kisaka et al. 2016). In this case the peak time of the light curve is determined by that of the energy injection, not by the diffusion.

where E is the total injected energy, t_e is the injection timescale, and ℓ is the decay index. We describe continuous injection models by $t_e \gtrsim t_d$ or $\ell \leq 2$. We use $\ell = 2$ for a magnetar model and $\ell = 5/3$ for a TDE model.

In principle, the above parameters can be derived from the observed bolometric light curve. Explosive injection models show a characteristic light curve with time dependence $\propto e^{-t^2/2t_d^2}$ as in the first term of Equation (6), i.e., the light curve is flat up to the diffusion time t_d and then it decays exponentially.⁸ On the other hand, continuous injection models yield a rising light curve up to the diffusion time t_d and a power-law decay afterward. Figure 1 depicts several examples that will be discussed in detail in Section 3. It is worth noting, however, that the bolometric light curve around the peak ($t \approx t_d$) is insensitive to the time dependence of the energy injection because of the convolution with a Gaussian function in Equation (6). Therefore, there is a significant degeneracy among the models if the observed bolometric light curve is known only around the peak.

Figure 1 shows the bolometric light curve of the SN-like bump (SN 2011kl) associated with the *u*/GRB 111209A (G15). Apparently, according to G15, these observations show a rising light curve, favoring a continuous energy injection as in a magnetar or TDE rather than an explosive model. The late-time data have errors that are too large to distinguish between a power law (corresponding to a continuous injection) and an exponential decay (corresponding to an explosive injection). G15 extract the SN-like bump component by subtracting the contributions of the afterglow and the host galaxy from the total light curve, as reproduced in Figure 2 (see Section 3.2 for details). G15 adopt a broken power-law afterglow,

$$F_\nu \propto \nu^{-\frac{p-1}{2}} \left[(t/t_0)^{q\lambda_1} + (t/t_0)^{q\lambda_2} \right]^{-1/q}, \quad (8)$$

where $\lambda_1 = 1.55$, $\lambda_2 = 2.33$, and $t_0 = 9.12 \text{ d}$ in the observer frame. In Figure 2, we use $q = 3$ (where larger q values give sharper breaks), and a spectral index $p = 2.6$ (Stratta et al. 2013).

However, the conclusion supporting continuous energy injection depends on the light curve modeling of the afterglow of the *u*/GRB 111209A. If we adopt a single (unbroken) power law for the optical afterglow,

$$F_\nu \propto \nu^{-\frac{p-1}{2}} (t/t_0)^{\lambda_3}, \quad (9)$$

the bolometric light curve will be initially flat, as shown by open circles⁹ in Figure 1. This instead favors an explosive injection rather than a continuous one. Here we use $\lambda_3 = 2$, and 0.7 mag fainter normalization at $t = t_0$ than in the broken case, as shown in Figure 3 (see Section 3.1 for details). This choice of parameters reduces the contribution of the afterglow at rest-frame $t \lesssim 10$ days and therefore enhances the contribution of the SN-like signal during the initial phase. Although G15 mention that “the afterglow light curve shows clear evidence for a steeper afterglow decay at > 10 days post-burst,

⁸ The shape of the light curve depends weakly on the density profile of the ejecta, which is not taken into account in our one-zone analysis (see, e.g., Rabinak & Waxman 2011 for discussions). In Figure 3, the multi-band light curves are not flat because the temperature is changing.

⁹ To obtain the open circles in Figure 1, we add the difference between Equations (8) and (9) to the bolometric light curve of G15.

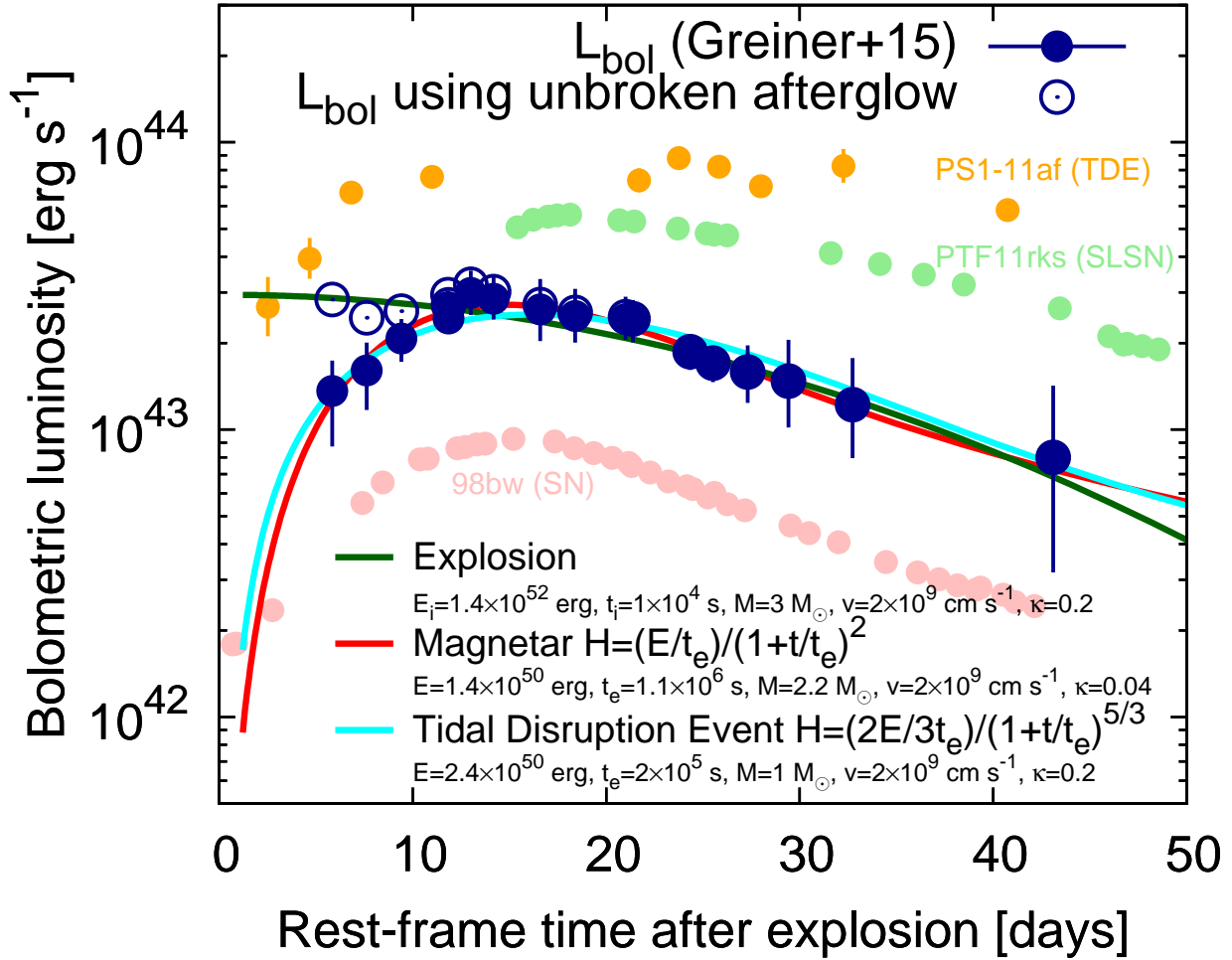


FIG. 1.— Bolometric light curve of the SN-like bump (SN 2011kl) associated with the *u*GRB 111209A with 1σ error bars (blue), integrated over rest-frame wavelengths of 230–800 nm, with the broken afterglow in Equation (8) and host galaxy components subtracted from the total light curve (G15). We also show the same bolometric light curve by using the unbroken afterglow in Equation (9) instead of the broken afterglow (open circle). The former light curve favors a continuous energy injection such as the magnetar model (red curve; $H = \frac{E/t_e}{[1+(t/t_e)]^2}$ with $E = 1.4 \times 10^{50}$ erg, $E_i = 0$ erg, $t_e = 1.1 \times 10^6$ s, $M = 2.2M_\odot$, $v = 2 \times 10^9$ cm s $^{-1}$, $\kappa = 0.04$) and the TDE model (cyan curve; $H = \frac{2E/3t_e}{[1+(t/t_e)]^{5/3}}$ with $E = 2.4 \times 10^{50}$ erg, $E_i = 0$ erg, $t_e = 2 \times 10^5$ s, $M = 1M_\odot$, $v = 2 \times 10^9$ cm s $^{-1}$, $\kappa = 0.2$), while the latter one prefers explosive energy injection such as the blue supergiant model (green curve; the first term in Equation (6) with $E_i = 1.4 \times 10^{52}$ erg, $E = 0$ erg, $t_i = 1 \times 10^4$ s, $M = 3M_\odot$, $v = 2 \times 10^9$ cm s $^{-1}$, $\kappa = 0.2$). For comparison, we also plot SN 1998bw/GRB 980425 (Galama et al. 1998), SLSN PTF11rks (Inserra et al. 2013), and TDE PS1-11af (Chornock et al. 2014).

particularly in the u' -band, where there is essentially no contribution from the supernova” (see also Kann et al. (2016)), such a break is apparently buried in fluctuations and errors of the flux, and the presence of a break in the u' -band seems unclear in Figures 2 and 3 (see Section 3 for implications of the X-ray light curve). Moreover, the optical afterglow has a large brightening at ~ 1 day, implying the existence of significant fluctuations in flux.

In summary, the bolometric light curve of the SN-like bump in *u*GRB 111209A does not provide conclusive evidence as to whether the energy injection is explosive or continuous because the initial light curve may be either rising or flat depending on the afterglow modeling, and the exact shape of the late decay has large errors.

As shown in Section 3.1, the energy required in an explosive injection is $E_i \sim 10^{52}(vt_i/2 \times 10^{13} \text{ cm})^{-1}$ erg,

most of which is adiabatically cooled. This inefficiency limits the size of the progenitor to $vt_i > 10^{13}$ cm, suggesting a supergiant.

3. MULTI-BAND LIGHT CURVES OF THE SUPERNOVA-LIKE BUMPS

We consider now specific models for *u*GRBs: a blue supergiant collapsar, a magnetar, and a WD-TDE. We reproduce the expected optical/near-infrared light curves of the SN-like bump associated with the *u*GRB 111209A in Figures 3, 2, and 4, respectively.

The multi-band light curves are calculated using Equations (6) and (7), with parameters ($\ell, E, t_e, M, v, \kappa, E_i = 0$) or ($E_i, t_i, M, v, \kappa, E = 0$) that are specified for each model below, and by multiplying the bolometric flux by

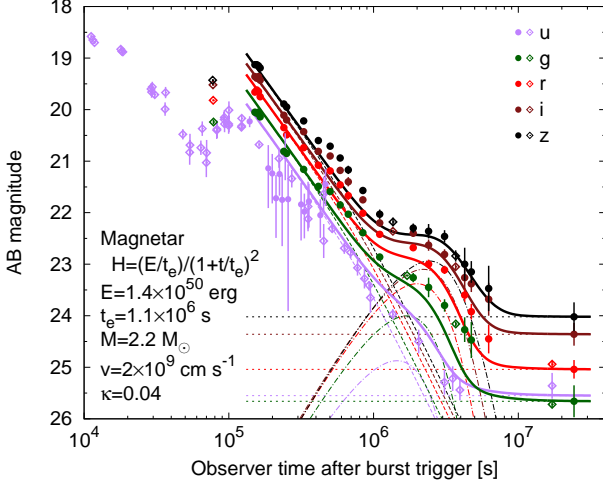


FIG. 2.— The optical/near-infrared u, g, r, i, z -band light curves of the u GRB 111209A by using a magnetar model in Equations (6), (7), and (10) with the decay index $\ell = 2$, the total injected energy $E = 1.4 \times 10^{50}$ erg, $E_i = 0$ erg, the energy injection time $t_e = 1.1 \times 10^6$ s, the ejecta mass $M = 2.2 M_\odot$, the ejecta velocity $v = 2 \times 10^9$ cm s $^{-1}$, and the opacity $\kappa = 0.04$. A broken afterglow in Equation (8) is utilized. The constant host galaxy contribution is accurately determined at late times. Data points are g', r', i', z' -band observations with GROND in Extended Data Table 1 of G15, u -band observations with *Swift*/UVOT in Extended Data Table 2 of G15, U and White-band observations with *Swift*/UVOT in Table 4 of Levan et al. (2014), and ground-based u, g, r, i, z -band observations in Table 8 of Levan et al. (2014). The magnetar model reproduces the multi-band observations within the fluctuations and errors of the flux.

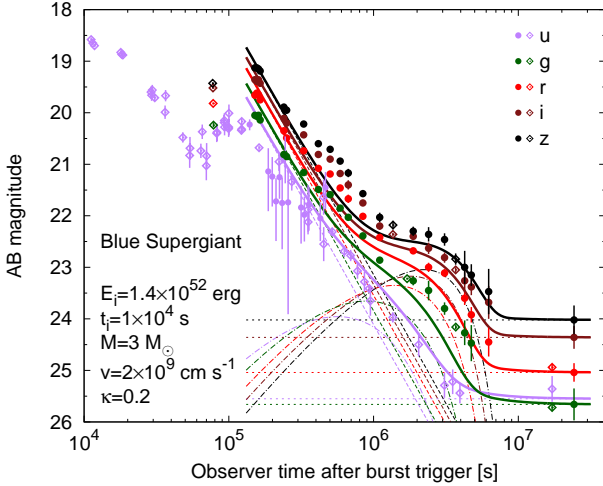


FIG. 3.— The same as Figure 2 except for the use of a blue supergiant model with $E_i = 1.4 \times 10^{52}$ erg, $E = 0$ erg, $t_i = 1 \times 10^4$ s, $M = 3 M_\odot$, $v = 2 \times 10^9$ cm s $^{-1}$, and $\kappa = 0.2$ in the first term of Equation (6) and Equation (10), and an unbroken afterglow in Equation (9). The blue supergiant model also reproduces the multi-band observations within the fluctuations and errors of the flux. For the data points, see the caption of Figure 2.

the black-body factor $\pi B_\nu / \sigma T^4$ where

$$T = \left(\frac{L}{4\pi\sigma v^2 t^2} \right)^{1/4}, \quad B_\nu = \frac{2h\nu^3/c^2}{\exp(h\nu/k_B T) - 1}. \quad (10)$$

We then convert the flux f_ν [erg s $^{-1}$ cm $^{-2}$ Hz $^{-1}$] to the

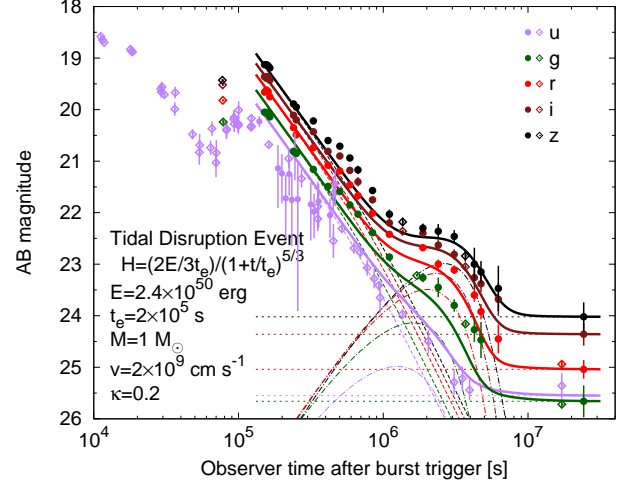


FIG. 4.— The same as Figure 2 except for the use of a WD-TDE model with $\ell = 5/3$, $E = 2.4 \times 10^{50}$ erg, $E_i = 0$ erg, $t_e = 2 \times 10^5$ s, $M = 1 M_\odot$, $v = 2 \times 10^9$ cm s $^{-1}$, and $\kappa = 0.2$ in Equations (6), (7) and (10). The same broken afterglow in Equation (8) is utilized as in Figure 2. The WD-TDE model also reproduces the multi-band observations within the fluctuations and errors of the flux. For the data points, see the caption of Figure 2.

AB magnitude m_{AB} using $m_{AB} = -\frac{5}{2} \log_{10} f_\nu - 48.6$. We adopt $A_V^{\text{Gal}} = 0.06$ mag Galactic foreground extinction¹⁰ and the host galaxy extinction with rest-frame $A_V^{\text{Host}} = 0.12$ mag assuming SMC-type dust (Pei 1992).¹¹

As discussed in Section 2.2, the strong afterglow at early times makes it difficult to distinguish between an explosive and a continuous energy injection. The X-ray afterglow observed by *Swift*/XRT does not show a jet break until $\sim 2 \times 10^6$ s (Gendre et al. 2013; Levan et al. 2014), implying a single power law as in Equation (9). If we use the standard afterglow theory (Sari et al. 1998; Nakauchi et al. 2013; Stratta et al. 2013), the SN-like component has a flat initial phase (see Figure 1), suggesting an explosive energy injection like a blue supergiant collapsar. To obtain an initially rising light curve, we must use a broken power law as in Equation (8), which requires another source for the X-ray emission. This is possible if the central engine activity is long-lasting, at least until $\sim 2 \times 10^6$ s with a single power law.

3.1. A blue supergiant Collapsar

In a blue supergiant collapsar a relativistic jet is launched from an accreting BH formed during the gravitational collapse of a blue supergiant progenitor (Kashiyama et al. 2013; Nakauchi et al. 2013). The duration is much longer than that of canonical GRBs because the radius of a blue supergiant is much larger than that of an envelope-less star such as a Wolf-Rayet star, the typical long GRB progenitor (Suwa & Ioka 2011). While crossing the stellar envelope, the jet injects energy into the shocked matter, producing a

¹⁰ Following G15, $A_u = 0.085$ mag, $A_{g'} = 0.066$ mag, $A_{r'} = 0.046$ mag, $A_{i'} = 0.034$ mag, and $A_{z'} = 0.025$ mag.

¹¹ The host galaxy extinction at a wavelength λ is given by $A_\lambda = A_V^{\text{Host}} + \frac{E_\lambda - V}{E_B - V} E_{B-V}$ where $\frac{E_\lambda - V}{E_B - V}$ is given by Equation (5) in Pei (1992) and $E_{B-V} = A_V^{\text{Host}} / R_V$ with R_V in Table 2 of Pei (1992).

hot cocoon surrounding it (Begelman & Cioffi 1989; Ramirez-Ruiz et al. 2002; Matzner 2003; Bromberg et al. 2011b). Since the envelope is large, a significant amount of energy, of the order of the prompt GRB energy, is dissipated during this phase and is injected into the cocoon. After the jet breaks out, the hot cocoon expands. It transfers most of the energy to kinetic energy and the rest is released once the optical depth drops. This produces an SN-like component similarly to SNe IIP. The observed SN-like component in GRB 111209A is brighter than the energetic SN 1998bw/GRB 980425 (Galama et al. 1998) as shown in Figure 1. This may reflect the large envelope of a blue supergiant and the corresponding large energy of the cocoon.

We adopt the following parameters. We assume that the duration of the energy injection into the cocoon, t_i , is comparable to the duration of GRB 111209A. This is much shorter than the diffusion time t_d in Equation (1). As the energy injection is short-lived, we use only the first term in Equation (6). We assume a constant opacity $\kappa = 0.2 \text{ cm}^2 \text{ g}^{-1}$. The true opacity could differ in either direction by a factor of two: $\kappa \simeq 0.1 \text{ cm}^2 \text{ g}^{-1}$ for singly ionized helium, $\kappa \simeq 0.2 \text{ cm}^2 \text{ g}^{-1}$ for fully ionized helium, and $\kappa \simeq 0.4 \text{ cm}^2 \text{ g}^{-1}$ for fully ionized hydrogen. The remaining three parameters—the total injected energy $E_i = 1.4 \times 10^{52} \text{ erg}$, the ejecta mass $M = 3M_\odot$, and the ejecta velocity $v = 2 \times 10^9 \text{ cm s}^{-1}$ —are chosen to fit the flux, timescale, and temperature (or multi-band data) of the SN-like bump (see Equations (1) and (2)).

Figure 3 shows a comparison between the observations and the model light curves. The blue supergiant collapsar reproduces the multi-band observations within the fluctuations and errors of the flux, and it is consistent with the multi-band light curves of GRB 111209A.¹²

A natural feature of this model is that the kinetic energy of the ejecta, $E_k = 1.2 \times 10^{52} \text{ erg} (M/3M_\odot)(v/2 \times 10^9 \text{ cm s}^{-1})^2$, is almost equal to the total injected energy $E_i = 1.4 \times 10^{52} \text{ erg}$. In turn, this energy, E_i , is the energy given by the jet to the cocoon (Bromberg et al. 2011b). Assuming that the jet luminosity L_j within the envelope is the same as that of the *u*/GRB, this energy is estimated as (Bromberg et al. 2011b)

$$E_i = L_j t_i = L_j T_{90} \left(\frac{t_i}{T_{90}} \right) = E_{\gamma, \text{iso}} \left(\frac{\theta_j^2}{\epsilon_\gamma} \right) \left(\frac{t_i}{T_{90}} \right) \quad (11)$$

where $E_{\gamma, \text{iso}} \sim 5.2 \times 10^{52} \text{ erg}$ is the observed isotropic gamma-ray energy (Levan et al. 2014), the jet duration t_i is of the order of $2 \times 10^{13} \text{ cm} / 0.1c \approx 6000 \text{ s}$, θ_j ($\gtrsim 0.2$ radian for the absence of a jet break) is the opening angle of the jet, and ϵ_γ is the radiative efficiency, which is of the order of 0.1–0.2. With these parameters the factor multiplying $E_{\gamma, \text{iso}}$ is ~ 0.2 , yielding the required E_i . Note that the two energies, E_k and E_i (or E in Equation (7)), which are comparable in this case, are very different in the other models as shown below.

3.2. A magnetar

When discussing magnetars, we have to distinguish between an “explosive” magnetar and a “continuous” magnetar. An explosive magnetar is one that operates on a short time scale (compared to the diffusion time), and in this case it is basically the same as the blue supergiant collapsar discussed in the previous section. To avoid significant adiabatic cooling and an excessive energy budget for the magnetar, it must involve a supergiant progenitor. In this case the magnetar could also produce the observed ultra-long prompt emission. The energy injection time can be comparable to the ultra-long prompt timescale (but this is also longer than and different from the standard central engines for GRB magnetars, which are about 100 s).

A “continuous” magnetar, i.e., a magnetar of G15, is one in which the energy release is comparable to the diffusion time scale. In the following we discuss the production of the SN-like bump by a continuous magnetar of this kind.

A millisecond magnetar—a highly spinning neutron star with a strong magnetic field—has been proposed as a possible central engine of GRBs (Usov 1992; Thompson & Duncan 1993; Wheeler et al. 2000; Thompson et al. 2004). The rotational energy of the neutron star is extracted by a relativistic wind of magnetized electron-positron plasma, which may lead to a relativistic jet for GRBs. The spin-down time of the dipole emission, t_s , is

$$t_s = \frac{6Ic^3}{B^2 R_{\text{NS}}^6 \Omega_i^2} \sim 1.6 \times 10^4 \text{ s} \left(\frac{B}{1 \times 10^{15} \text{ G}} \right)^{-2} \left(\frac{P_i}{2 \text{ ms}} \right)^2, \quad (12)$$

where I , R_{NS} , and $\Omega_i = 2\pi/P_i$ are the moment of inertia, radius, and angular velocity of a neutron star. This is adjustable to the required duration of the GRB. The total energy is chosen to be larger than the observed released energy.

The model is flexible so as to accommodate, by tuning P_i and B , diverse transients (Metzger et al. 2015; Kashiyama et al. 2016). In particular, magnetars have been applied to possible central engines of GRBs on a time scale of tens of seconds or even shorter for *s*GRBs (Usov 1992; Thompson & Duncan 1993; Wheeler et al. 2000; Thompson et al. 2004), including low-luminosity GRBs (e.g., Mazzali et al. 2006; Toma et al. 2007), and the afterglow X-ray plateaus on a time scale of a few hours (e.g., Corsi & Mészáros 2009). Additionally, magnetars have been proposed to power SLSNe¹³ on a time scale of a few weeks (Kasen & Bildsten 2010; Woosley 2010; Metzger et al. 2015; Mösta et al. 2015; Kashiyama et al. 2016). Although the SN-like bump of the *u*/GRB 111209A is fainter than typical SLSNe by more than one magnitude, and the spectrum of GRB 111209A is more featureless than that of SLSNe, a magnetar has been put forward as a possible energy source for the observed SN-like bump (G15).

¹² Our light curve modeling is different from that of Nakauchi et al. (2013), who include the large brightening at ~ 1 day in the model fitting. We think that this is not appropriate given the GROND data (G15).

¹³ In particular, hydrogen-poor (Type I) SLSNe are difficult to explain by radioactivity or interaction with circumstellar material, and hence the energy injection from the central engine magnetar to the supernova ejecta has been suggested as the mechanism that makes these SLSNe so bright (Gal-Yam 2012).

We adopt the following parameters to calculate the light curve of the magnetar-powered emission $L(t)$: the decay index of the energy injection $H(t)$ is determined by the spin-down index $\ell = 2$. We adopt the same ejecta mass $M = 2.2M_\odot$ and velocity $v = 2 \times 10^9 \text{ cm s}^{-1}$ as in G15. The remaining three parameters—the energy injection time $t_e = 1.1 \times 10^6 \text{ s}$, the total injected energy $E = 1.4 \times 10^{50} \text{ erg}$, and the opacity $\kappa = 0.04$ —are chosen to fit the peak time, height, and shape (width) of the light curve (see Equations (1) and (2)). Note that t_e , E , and κ are not written explicitly in G15, but these three parameters are fixed by the choice of M and v and the three observables—the peak time, height, and width of the light curve.

Figure 2 reproduces the model described by G15 (see also Kann et al. (2016)) and shows a comparison between the observations and the model light curves. The model is consistent with the multi-band light curves of the *u*/GRB 111209A within the fluctuations and errors of the flux.

While the light curve can be fitted by this model of energy injection, the magnetar model as a whole has several problems. First, there is a tension between the properties of the prompt emission and those required for the production of the SN-like bump. The energy injection time $t_e = 1.1 \times 10^6 \text{ s}$ is determined by the peak time of $\sim 10^6 \text{ s}$ of the SN-like bump. If we identify t_e with the spin-down time of the magnetar, it is different from the duration of *u*/GRB 111209A by two orders of magnitude. To explain both the prompt emission and the late SN-like bump within a magnetar model, we require a peculiar behavior: the magnetic field should be initially large, leading to a relatively faster decay, but then it should change sometime between the prompt emission and the SN-like bump. This is possible, but it requires an ad hoc assumption that does not arise naturally. Furthermore, it is puzzling why this behavior is observed here and not in other cases. Note that Metzger et al. (2015) and Bersten et al. (2016) adopted a spin-down time comparable to the GRB duration of $\sim 10^4 \text{ s}$, but this choice of parameter makes the bolometric light curve decay too rapidly after the peak. This is exactly the reason why Bersten et al. (2016) require some amount of ^{56}Ni to fit the light curve. Cano et al. (2016) adopt a spin-down time similar to ours and introduce a power-law component to fit the fast decay phase after the prompt emission, but in this case they cannot explain the GRB duration by the magnetar activity, and yet another central engine has to be invoked to explain that.

Second, the kinetic energy $\sim 10^{52} \text{ erg}$ of the ejecta given now by Equation (3) is much larger than the total injected energy $E = 1.4 \times 10^{50} \text{ erg}$. This means that the magnetar releases most of its energy, $\sim 10^{52} \text{ erg}$, at a very early time and injects a moderate energy $\sim \frac{1}{2} I \Omega_i^2 \sim 10^{50} \text{ erg}$ later at $t_e \sim 10^6 \text{ s}$ for the SN-like activity. This again requires an unnatural behavior of magnetic fields. Although this behavior is consistent, a fair fraction of the prompt energy has to be transferred to the kinetic energy, probably requiring an extended envelope as in Equation (11). In addition, the X-ray afterglow does not show a break at $\sim 1 \times 10^6 \text{ s}$, which is not fully consistent with the required injection time t_e .

Third, the required opacity $\kappa \sim 0.04$ is relatively small

for ordinary ionized plasma, even though the spectra suggest a low metal content with 1/4 of the solar metallicity (G15; Mazzali et al. 2016). This problem is also pointed out by Bersten et al. (2016). For larger opacity $\kappa \gtrsim 0.1$, a smaller ejecta mass $M \lesssim 1M_\odot$ is required because κ appears as the combination κM in the diffusion time t_d in Equation (1), but such a small ejecta mass is unlikely for a newborn magnetar.

Finally, it is not clear what is the mechanism that converts the Poynting flux of the magnetar wind to heat that leads to the observed radiation. If the Poynting flux just exerts pressure on the ejecta, it will just accelerate it. A fraction of the Poynting energy would be converted into the thermal energy through shocks in the ejecta or reconnections of the magnetic fields, but the process and its efficiency are not known. The efficiency could be very different from that in the cases of radiation or matter (e.g., Bromberg et al. 2014). Note that in blue supergiant collapsars and WD-TDEs the initial energy (for collapsars) or the injected energy (for WD-TDEs) is transferred directly to the thermal energy.

In summary, the continuous magnetar model could be made consistent with the light curves of GRB 111209A. However, this happens by choosing somewhat unusual model parameters and requires either a varying magnetic field, with an order-of-magnitude jump, between the prompt *u*/GRB phase and the SN-like bump phase or a different GRB central engine. Although it is somewhat strange, clearly one cannot exclude this model.

3.3. A WD-TDE

A TDE of a WD is also a possible origin of *u*/GRBs (Gendre et al. 2013; Levan et al. 2014; MacLeod et al. 2014). A star is tidally disrupted when it passes near a BH (Rees 1988). The disruption occurs at a tidal radius $R_T \sim (3M_{\text{BH}}/4\pi\rho_*)^{1/3} \sim 4 \times 10^{10} \text{ cm}$ for a typical WD density $\rho_* \sim 10^6 \text{ g cm}^{-3}$ and a BH mass $M_{\text{BH}} \sim 10^5 M_\odot$. The disrupted bound matter is given elliptical trajectories with large apocenter distances, while unbound material moves on hyperbolic orbits. The most bound matter has a semimajor axis

$$a_{\text{min}} \sim \left(\frac{M_{\text{BH}}}{M_*} \right)^{1/3} R_T \sim 2 \times 10^{12} \text{ cm} \left(\frac{M_{\text{BH}}}{10^5 M_\odot} \right)^{2/3} \times \left(\frac{M_*}{1M_\odot} \right)^{-1/3} \left(\frac{\rho_*}{10^6 \text{ g cm}^{-3}} \right)^{-1/3} \quad (13)$$

for the stellar mass $M_* \sim 1M_\odot$, with an orbital time

$$t_0 \sim 2\pi \sqrt{\frac{a_{\text{min}}^3}{GM_{\text{BH}}}} \sim 4 \times 10^3 \text{ s} \left(\frac{M_{\text{BH}}}{10^5 M_\odot} \right)^{1/2} \times \left(\frac{M_*}{1M_\odot} \right)^{-1/2} \left(\frac{\rho_*}{10^6 \text{ g cm}^{-3}} \right)^{-1/2}. \quad (14)$$

If the BH accretes the fallback matter and launches a jet, the WD-TDE model can explain the duration of *u*/GRBs. Here a WD is essential because a regular star provides too long a timescale (Krolik & Piran 2011), which would be inconsistent with the observed variability of the prompt phase of this event.

WD-TDEs were suggested by Krolik & Piran (2011)¹⁴ when Swift J1644+57 was discovered as luminous X-ray flares over several days (Bloom et al. 2011; Burrows et al. 2011; Levan et al. 2011; Zauderer et al. 2011). The flux decay $t^{-5/3}$ after $\sim 10^6$ s as well as the location close to the nucleus of a galaxy indicate a TDE. The observed variability on a timescale of a few hundred seconds implied that the disrupted object is a WD and not a regular star. The latter would imply a minimal variability timescale of the order of 10^4 s. The super-Eddington luminosity and non-thermal spectrum strongly suggest that the TDE launches a relativistic jet. So far several similar events have been discovered such as Swift J2058+0516 (Cenko et al. 2012) and Swift J1112-8238 (Brown et al. 2015). Their different X-ray characteristics as compared with optical TDE candidates suggest that their accretion physics is different, either due to the different disrupted star or due to a different geometry, and that in these cases an efficient accretion results in the formation of a jet that produces the X-ray emission.

u /GRBs have several similarities to Swift J1644+57:¹⁵

1. The flux decay is close to, if not exactly the same as, $t^{-5/3}$, as shown in Table 1, where we note that the decay index is subject to change as a result of the choice of the origin of time.
2. The peak luminosities, $\sim 10^{49}$ erg s⁻¹, of u /GRBs are higher than those of Swift J1644+57 and Swift J2058+0516, but the differences are only one or two orders of magnitude, much smaller than the diversity of GRB luminosities (see Figure 15 in Evans et al. 2014).
3. The differences in duration are also at the same level as the luminosities (see Figure 15 in Evans et al. 2014).
4. The locations of u /GRBs for which data are available (GRB 101225A, GRB 111209A, and GRB 130925A) are consistent with the nuclei of the host galaxies (see Section 5 for further details).

In addition, theoretical estimates of the WD-TDE rate (Krolik & Piran 2011; Shcherbakov et al. 2013; MacLeod et al. 2014) are consistent with the u /GRB rate ~ 1 Gpc⁻³ yr⁻¹ (Levan et al. 2014), taking the numerous uncertainties into account.

In view of the observed SN-like bump in GRB 111209A, G15 discarded the WD-TDE model. However, it is premature to do so because the SN-like bump can be easily powered by the material falling back onto the massive BH. Half of the stellar mass falls back and the other half is ejected to infinity (see Figure 5). The fallback mass $\sim M_*/2$ first dissipates its gravitational energy via shocks between tidal streams at the outer radius of the most bound orbit, $\sim a_{\min}$ in Equation (13), much further than the tidal radius R_T , as suggested

by the optical TDEs (Piran et al. 2015) and simulations (Shiokawa et al. 2015). The energy dissipated at the radius a_{\min} ,

$$E \sim \frac{GM_{\text{BH}}(M_*/2)}{2a_{\min}} \sim 4 \times 10^{51} \text{ erg} \left(\frac{M_{\text{BH}}}{10^5 M_\odot} \right)^{1/3} \times \left(\frac{M_*}{1 M_\odot} \right)^{4/3} \left(\frac{\rho_*}{10^6 \text{ g cm}^{-3}} \right)^{1/3}, \quad (15)$$

is comparable to the energy required for the SN-like bump (see Sec. 2.1 and below). Furthermore, an even larger amount of energy can be released as the matter accretes closer to the BH. The dissipation lasts for the circularization timescale of the fallback matter, which is longer than the orbital time $t_0 \sim 4 \times 10^3$ s given by Equation (14) by at least a factor of 5–10 (Piran et al. 2015; Shiokawa et al. 2015). While the accretion can be inefficient at this stage (Svirski et al. 2015), the overall accretion rate is super-Eddington. If the accretion is efficient, it will lead to a strong disk emission in the UV and soft X-rays (see Piran et al. 2015)¹⁶ or to a powerful outflow via radiation pressure (Ohsuga et al. 2005; Strubbe & Quataert 2009; Metzger & Stone 2016). The emission or outflow is surrounded by the optically thick tidal ejecta, so that the resulting energy is injected into the ejecta. The injected energy is radiated later via diffusion and thermalization, and appears to be an SN-like bump like SNe IIP (see Figure 5). The luminosity is regulated by the optically thick ejecta down to the Eddington luminosity of the BH (Shen et al. 2016):

$$L_{\text{Edd}} \sim 10^{43} \text{ erg s}^{-1} \left(\frac{M_{\text{BH}}}{10^5 M_\odot} \right), \quad (16)$$

which is close to the observed one. The required ejecta mass $\sim 1 M_\odot$ (see Section 2.1) is consistent within the model uncertainties. In addition, the escape velocity at $\sim a_{\min}$,

$$v_{\min} \sim \sqrt{\frac{GM_{\text{BH}}}{2a_{\min}}} \sim 2 \times 10^9 \text{ cm s}^{-1} \left(\frac{M_{\text{BH}}}{10^5 M_\odot} \right)^{1/6} \times \left(\frac{M_*}{1 M_\odot} \right)^{1/6} \left(\frac{\rho_*}{10^6 \text{ g cm}^{-3}} \right)^{1/6}, \quad (17)$$

which is of the same order as the velocity of the unbound material, gives the right value for the observed ejecta velocity (see Sec. 2.1 and below). Therefore a WD-TDE can naturally explain the SN-like bump observed in GRB 111209A. Note that the mechanism of the energy injection into the ejecta proposed here is different from the previous proposals, such as optical flares from the TDE (Bogdanovic et al. 2004; Strubbe & Quataert 2009; Clausen & Eracleous 2011)¹⁷ and a thermonuclear SN I by tidal compression of the WD (Luminet & Pichon 1989; Rosswog et al. 2008, 2009; MacLeod et al. 2014, 2016). Metzger & Stone (2016) consider a similar mechanism to ours for optical TDEs, although the energy is

¹⁴ These events have been suggested also as possible progenitors of SNe Ia (Luminet & Pichon 1989; Rosswog et al. 2008, 2009).

¹⁵ An optical/IR bump is associated with Swift J1644+57 (Levan et al. 2016), but it is not clear whether this is the same phenomenon as the SN-like bump in GRB 111209A or just the afterglow rebrightening.

¹⁶ Piro et al. (2014) and Bellm et al. (2014) detected a thermal X-ray component in the u /GRB 130925A, but their estimates of the emission size are different, and it is not clear whether the X-rays are relevant to the disk emission or not.

¹⁷ They considered the reprocessed emission by unbound matter, but only lines, not continuum.

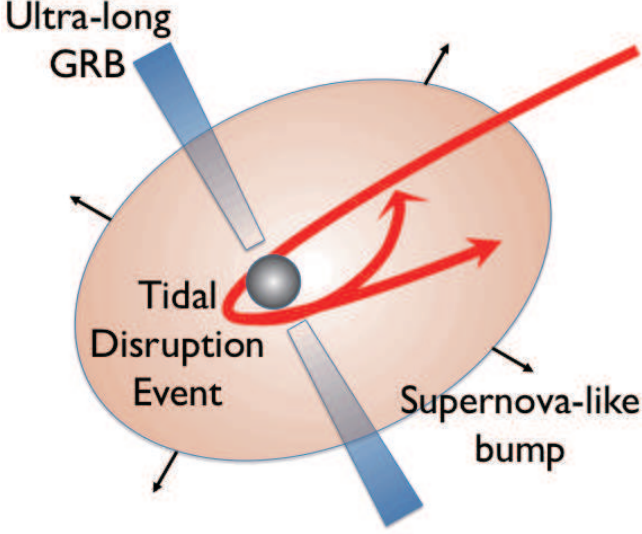


FIG. 5.— Schematic picture of a TDE associated with a *ul*GRB jet as well as SN-like ejecta. The SN-like ejecta is powered by the gravitational energy of the fallback matter, which is transferred to the surrounding ejecta via shocks or radiation. The ejecta releases the injected energy after expansion, making the SN-like bump like SNe IIP (see text for details).

released at the pericenter by a small fraction of the matter accretion (not at the apocenter by half of the matter accretion).

We choose the following parameters to calculate the light curve of the WD-TDE emission $L(t)$: the decay index of the energy injection $H(t)$ is determined by the fallback index $\ell = 5/3$ (Rees 1988; Phinney 1989). We adopt $\kappa = 0.2 \text{ cm}^2 \text{ g}^{-1}$ for fully ionized carbon and oxygen (e.g., Piro & Morozova 2014). The mass $M = 1M_\odot$ and velocity $v = 2 \times 10^9 \text{ cm s}^{-1}$ are taken according to Section 2.1. The remaining two parameters—the total injected energy $E = 2.4 \times 10^{50} \text{ erg}$ and energy injection time $t_e = 2 \times 10^5 \text{ s}$ —are chosen to fit the peak height and the shape (width) of the light curve.

Figure 4 shows a comparison between the observations and the TDE model. The model reproduces the multi-band light curves of *ul*GRB 111209A within the fluctuations and errors of the flux.

The implications of the required model parameters for the WD-TDE model are as follows. First, the energy injection time $t_e = 2 \times 10^5 \text{ s}$ is longer than the orbital time $t_0 \sim 4 \times 10^3 \text{ s}$. This may be natural because the circularization process of the fallback matter is rather slow, lasting at least $\sim 5\text{--}10t_0$ as found in numerical simulations (Shiokawa et al. 2015) and suggested by optical TDEs (Piran et al. 2015). Note that the observed X-ray afterglow most likely arises from a jet, whose origin is different from the process that produces that powers the SN-like bump. Second, the kinetic energy $E_k \sim \frac{1}{2}Mv^2 \sim 4 \times 10^{51} \text{ erg}$ of the ejecta is larger than the total injected energy $E = 2.4 \times 10^{50} \text{ erg}$. This is natural because the kinetic energy in this case is just the original kinetic energy of the unbound stellar debris and it is not related to the process that heats the outflow at a later time, causing the observed emission.

4. THE SPECTRUM OF THE SUPERNOVA-LIKE BUMP

The absence of hydrogen lines from the SN-like emission of the *ul*GRB 111209A is used by G15 to rule out a blue supergiant progenitor. Carbon and oxygen lines are also not observed, contrary to the expectation of a WD-TDE (Clausen & Eracleous 2011), although radiation transfer modeling suggests that the composition is consistent with the carbon-oxygen cores of massive stars (Mazzali et al. 2016). In any case, as we will show below, these elements could be ionized by radiation, and thus would not display these lines.

The observed X-ray emission at the peak of the SN-like bump ~ 10 days after GRB 111209A has a luminosity $L_X \sim 10^{44} \text{ erg s}^{-1}$. The emission likely comes from the central engine for the WD-TDE model (see Section 3.3). Although the observed X-ray emission may be an afterglow for the blue supergiant model, the central engine could expose itself at the late time of ~ 10 days and the emission could be comparable to that observed. The X-rays ionize the ejecta, which is composed, for example, of oxygen ($Z = 8Z_8$), at a rate $t_{\text{ion}}^{-1} = n_\gamma \sigma_i c$ where $n_\gamma = L_X / 4\pi R^2 c h \nu$ is the number density of ionizing photons, $\sigma_i = 1 \times 10^{-19} Z_8^{-2} \text{ cm}^2$ is the ionization cross section, and $h\nu = 871 Z_8^2 \text{ eV}$ is the ionization energy (Osterbrock & Ferland 2006; Metzger et al. 2014). On the other hand, the recombination rate is $t_{\text{rec}}^{-1} = n_e \alpha_{\text{rec}}$ where $n_e \simeq \rho / 2m_p$ is the electron density, $\rho = 3M / 4\pi R^3$ is the density of the ejecta, and $\alpha_{\text{rec}} \sim 2 \times 10^{-11} Z_8^2 T_4^{-0.8} \text{ cm}^3 \text{ s}^{-1}$ is the case B recombination coefficient (Osterbrock & Ferland 2006; Metzger et al. 2014). We find that the ionization dominates the recombination,

$$\frac{t_{\text{rec}}}{t_{\text{ion}}} = \frac{n_\gamma \sigma_i c}{n_e \alpha_{\text{rec}}} \sim 2 \times 10^2 Z_8^{-6} T_4^{0.8} \left(\frac{L_X}{10^{44} \text{ erg s}^{-1}} \right) \times \left(\frac{v}{10^9 \text{ cm s}^{-1}} \right) \left(\frac{t}{10 \text{ d}} \right) \left(\frac{M_{\text{ej}}}{1M_\odot} \right)^{-1}, \quad (18)$$

where the ionization parameter is given by

$$\frac{n_\gamma}{n} \sim \frac{n_\gamma}{n_e / Z} \sim 9 Z_8^{-1} \left(\frac{L_X}{10^{44} \text{ erg s}^{-1}} \right) \left(\frac{v}{10^9 \text{ cm s}^{-1}} \right) \times \left(\frac{t}{10 \text{ d}} \right) \left(\frac{M_{\text{ej}}}{1M_\odot} \right)^{-1}. \quad (19)$$

Therefore hydrogen, carbon, and oxygen in the ejecta could be ionized by X-rays. The absence of these lines rejects neither the blue supergiant model nor the WD-TDE model.

As similar examples, hydrogen lines have recently been observed in the late-time spectra of a hydrogen-poor SLSN (Yan et al. 2015). Helium lines have also appeared at a later stage in SN 2008D (Mazzali et al. 2008). It is dangerous to conclude the absence of elements from incomplete observations of lines.

5. LOCATION IN HOST GALAXIES

The location in the host galaxies is an important clue to the identification of the origin of sources. Association with the nuclei of the host galaxies implies TDEs by massive BHs. Currently we have astrometric data for GRB 101225A, GRB 111209A, and GRB 130925A as shown in Table 1. GRB 101225A and GRB 111209A lie within 150

and 250 pc of the nucleus, respectively. This is consistent with TDEs. However, these hosts are compact, making it difficult to draw a firm conclusion (Levan et al. 2014). GRB 130925A is slightly offset from the nucleus of the galaxy by ~ 600 pc, while the host galaxy is large with an effective radius of ~ 2.4 kpc (Schady et al. 2015).

The probability of all three bursts accidentally occurring close to the nuclei may be small, even though each case is not rare in itself. The probability of occurrence at a position $r < R_i$ in a galaxy with a (two-dimensional Gaussian) radius R_g is given by

$$P_i(R_i) = \int_0^{R_i/R_g} r e^{-r^2/2} dr = 1 - e^{-R_i^2/2R_g^2}, \quad (20)$$

where the radius R_g is related to $x\%$ light radius R_x by $P_i(R_x) = x\%$. With Table 1, we obtain the probability

$$P_{101225A} \cdot P_{111209A} \cdot P_{130925A} \simeq 0.0957 \cdot 0.186 \cdot 0.0424 \\ \simeq 0.000753. \quad (21)$$

This is $\simeq 3.4\sigma$ that and could indicate the WD-TDE model. Note that the compact nature of host galaxies for GRB 101225A and GRB 111209A also suggests a small mass of nuclear BHs (Levan et al. 2014), which is required for WD-TDEs.

6. SUMMARY AND DISCUSSIONS

We conclude that WD-TDE can naturally produce u GRBs that are accompanied by SN-like bumps. The fallback mass has enough gravitational energy to power both the u GRB and the SN-like bump. The WD mass and the velocity of unbound material are consistent with the ejecta mass and velocity required for the observed light curves of the SN-like bumps. The energy (Equation (15)) and velocity (Equation (17)) for the SN-like bump in the u GRB 111209A are consistent with a picture in which the fallback matter dissipates energy at the outer radius of the most bound orbit $\sim a_{\min}$ via mutual shocks between tidal streams. Part of the energy is absorbed by the optically thick ejecta, leading to the SN-like emission at the Eddington luminosity of the BH in Equation (16) as observed.

The locations of the bursts in the centers of their host galaxies are also favorable for a WD-TDE origin. By combining three events, for which data are available, the significance of concentration in nuclei is $\simeq 3.4\sigma$. These locations, of course, do not support the magnetar and blue supergiant collapsar models. The absence of carbon

and oxygen lines from the spectrum of the SN-like bump is not a problem since these elements can be ionized by the observed X-rays. Together with the flux decay close to $t^{-5/3}$ and a certain similarity to Swift 1644+57, the WD-TDE model is, to our minds, a strong candidate for the origin of u GRBs.

The observed SN-like bumps are also still consistent with the blue supergiant collapsar, and more broadly with an explosive injection model. The light curves of the SN-like bumps are subject to change due to the uncertainty of subtraction of the afterglow. Precise observations of multi-band light curves are necessary to distinguish whether the energy injection is explosive or continuous. The lack of hydrogen lines is not crucial evidence against the blue supergiant model since the observed level of X-rays can ionize hydrogen.

The physical parameters for reproducing the multi-band light curves for the magnetar model (i.e., a magnetar as in G15, not an explosive, short-lived magnetar; see Section 3.2), are not attractive. In particular, the required spin-down time of the magnetar is much longer than the prompt emission of u GRB 111209A. The location of u GRBs in host galaxies is also not consistent with that of SLSNe, which are possibly powered by magnetars. Nevertheless the magnetar model is still viable. Observations of the late-time decay are desirable to support or rule out this model. A further problem of this model is the need to convert the Poynting flux of the magnetar efficiently to heat that can be radiated away.

To conclude, we note that the WD-TDE model provides an interesting connection between u GRBs and BHs with masses less than $10^5 M_\odot$. Future observations of u GRBs and associated SN-like emission will probe intermediate-mass BHs if they are WD-TDEs. Off-axis u GRBs might be observed as SNe without GRBs in the SN surveys. Rapidly rising gap transients (Arcavi et al. 2016) are similar to the SN-like bump of u GRB 111209A, and their properties are interesting to study such as by searches for radio afterglow.

We would like to thank J. Greiner for providing information about the data used in G15, S. Kisaka for helpful discussions, and B. Metzger and an anonymous referee for helpful comments. This work is supported by SOKENDAI (The Graduate University for Advanced Studies), KAKENHI 24103006, 24000004, 26247042, 26287051 (K.I.), by an Israel Space Agency (SELA) grant and the I-Core center for excellence ‘‘Origins’’ of the CHE-ISF and by an adv ERC grant TREX.

REFERENCES

- Arcavi, I., Gal-Yam, A., Sullivan, M., et al. 2014, *ApJ*, 793, 38
 Arcavi, I., Wolf, W. M., Howell, D. A., et al. 2016, *ApJ*, 819, 35
 Arnett, W. D. 1979, *ApJ*, 230, L37
 —. 1980, *ApJ*, 237, 541
 Begelman, M. C., & Cioffi, D. F. 1989, *ApJ*, 345, L21
 Bellm, E. C., Barrière, N. M., Bhalerao, V., et al. 2014, *ApJ*, 784, L19
 Bersten, M. C., Benvenuto, O. G., Orellana, M., & Nomoto, K. 2016, *Astrophys. J.*, 817, L8
 Bloom, J. S., Giannios, D., Metzger, B. D., et al. 2011, *Science*, 333, 203
 Boer, M., Gendre, B., & Stratta, G. 2015, *Astrophys. J.*, 800, 16
 Bogdanovic, T., Eracleous, M., Mahadevan, S., Sigurdsson, S., & Laguna, P. 2004, *Astrophys. J.*, 610, 707
 Bromberg, O., Granot, J., Lyubarsky, Y., & Piran, T. 2014, *Mon. Not. Roy. Astron. Soc.*, 443, 1532
 Bromberg, O., Nakar, E., & Piran, T. 2011a, *ApJ*, 739, L55
 Bromberg, O., Nakar, E., Piran, T., & Sari, R. 2011b, *ApJ*, 740, 100
 Brown, G. C., Levan, A. J., Stanway, E. R., et al. 2015, *MNRAS*, 452, 4297
 Burrows, D. N., Kennea, J. A., Ghisellini, G., et al. 2011, *Nature*, 476, 421
 Campana, S., Lodato, G., D’Avanzo, P., et al. 2011, *Nature*, 480, 69
 Cano, Z., Johansson, A. K. G., & Maeda, K. 2016, *Mon. Not. Roy. Astron. Soc.*, 457, 2761
 Cenko, S. B., Krimm, H. A., Horesh, A., et al. 2012, *ApJ*, 753, 77

- Chornock, R., Berger, E., Gezari, S., et al. 2014, *ApJ*, 780, 44
- Clausen, D., & Eracleous, M. 2011, *ApJ*, 726, 34
- Corsi, A., & Mészáros, P. 2009, *ApJ*, 702, 1171
- Cucchiara, A., Veres, P., Corsi, A., et al. 2015, *ApJ*, 812, 122
- Dexter, J., & Kasen, D. 2013, *ApJ*, 772, 30
- Eichler, D., Livio, M., Piran, T., & Schramm, D. N. 1989, *Nature*, 340, 126
- Evans, P. A., Willingale, R., Osborne, J. P., et al. 2014, *MNRAS*, 444, 250
- Gal-Yam, A. 2012, *Science*, 337, 927
- Galama, T. J., Vreeswijk, P. M., van Paradijs, J., et al. 1998, *Nature*, 395, 670
- Gao, H., Lei, W.-H., You, Z.-Q., & Xie, W. 2016, *ApJ*, 826, 141
- Gao, H., & Mészáros, P. 2015, *Astrophys. J.*, 802, 90
- Gendre, B., Stratta, G., Atteia, J. L., et al. 2013, *ApJ*, 766, 30
- Greiner, J., et al. 2015, *Nature*, 523, 189
- Horesh, A., Cenko, S. B., Perley, D. A., et al. 2015, *ApJ*, 812, 86
- Inserra, C., Smartt, S. J., Jerkstrand, A., et al. 2013, *ApJ*, 770, 128
- Ioka, K. 2001, *MNRAS*, 327, 639
- Irwin, C. M., & Chevalier, R. A. 2016, *MNRAS*, 460, 1680
- Kann, D. A., Schady, P., Olivares E., F., et al. 2016, *ArXiv e-prints*, arXiv:1606.06791
- Kasen, D., & Bildsten, L. 2010, *ApJ*, 717, 245
- Kashiyama, K., Murase, K., Bartos, I., Kiuchi, K., & Margutti, R. 2016, *ApJ*, 818, 94
- Kashiyama, K., Nakauchi, D., Suwa, Y., Yajima, H., & Nakamura, T. 2013, *ApJ*, 770, 8
- Kisaka, S., Ioka, K., & Nakar, E. 2016, *ApJ*, 818, 104
- Krolik, J. H., & Piran, T. 2011, *ApJ*, 743, 134
- Kulkarni, S. R., Frail, D. A., Wieringa, M. H., et al. 1998, *Nature*, 395, 663
- Leloudas, G., Fraser, M., Stone, N. C., et al. 2016, *ArXiv e-prints*, arXiv:1609.02927
- Levan, A. J., Tanvir, N. R., Cenko, S. B., et al. 2011, *Science*, 333, 199
- Levan, A. J., Tanvir, N. R., Starling, R. L. C., et al. 2014, *ApJ*, 781, 13
- Levan, A. J., Tanvir, N. R., Brown, G. C., et al. 2016, *ApJ*, 819, 51
- Lien, A., Sakamoto, T., Barthelmy, S. D., et al. 2016, *ApJ*, 829, 7
- Luminet, J.-P., & Pichon, B. 1989, *A&A*, 209, 103
- MacFadyen, A., & Woosley, S. E. 1999, *Astrophys. J.*, 524, 262
- MacLeod, M., Goldstein, J., Ramirez-Ruiz, E., Guillochon, J., & Samsing, J. 2014, *ApJ*, 794, 9
- MacLeod, M., Guillochon, J., Ramirez-Ruiz, E., Kasen, D., & Rosswog, S. 2016, *ApJ*, 819, 3
- Matzner, C. D. 2003, *MNRAS*, 345, 575
- Mazzali, P. A., Sullivan, M., Pian, E., Greiner, J., & Kann, D. A. 2016, *MNRAS*, 458, 3455
- Mazzali, P. A., Deng, J., Nomoto, K., et al. 2006, *Nature*, 442, 1018
- Mazzali, P. A., Valenti, S., Della Valle, M., et al. 2008, *Science*, 321, 1185
- Metzger, B. D., Margalit, B., Kasen, D., & Quataert, E. 2015, *MNRAS*, 454, 3311
- Metzger, B. D., & Stone, N. C. 2016, *MNRAS*, 461, 948
- Metzger, B. D., Vurm, I., Hascoët, R., & Beloborodov, A. M. 2014, *MNRAS*, 437, 703
- Mösta, P., Ott, C. D., Radice, D., et al. 2015, *Nature*, 528, 376
- Murase, K., & Ioka, K. 2013, *Physical Review Letters*, 111, 121102
- Nagakura, H., Suwa, Y., & Ioka, K. 2012, *ApJ*, 754, 85
- Nakar, E. 2015, *ApJ*, 807, 172
- Nakauchi, D., Kashiyama, K., Suwa, Y., & Nakamura, T. 2013, *ApJ*, 778, 67
- Ohsuga, K., Mori, M., Nakamoto, T., & Mineshige, S. 2005, *Astrophys. J.*, 628, 368
- Osterbrock, D. E., & Ferland, G. J. 2006, *Astrophysics of gaseous nebulae and active galactic nuclei*
- Paczynski, B. 1998, *Astrophys. J.*, 494, L45
- Pei, Y. C. 1992, *ApJ*, 395, 130
- Perets, H. B., Li, Z., Lombardi, Jr., J. C., & Milcarek, Jr., S. R. 2016, *ApJ*, 823, 113
- Phinney, E. S. 1989, in *The Center of the Galaxy: Proceedings of the 136th Symposium of the International Astronomical Union*, ed. M. Morris (Dordrecht: Kluwer), 543
- Piran, T., Svirski, G., Krolik, J., Cheng, R. M., & Shiokawa, H. 2015, *ApJ*, 806, 164
- Piro, A. L., & Morozova, V. S. 2014, *ApJ*, 792, L11
- Piro, L., Troja, E., Gendre, B., et al. 2014, *ApJ*, 790, L15
- Rabinak, I., & Waxman, E. 2011, *ApJ*, 728, 63
- Ramirez-Ruiz, E., Celotti, A., & Rees, M. J. 2002, *MNRAS*, 337, 1349
- Rees, M. J. 1988, *Nature*, 333, 523
- Rosswog, S., Ramirez-Ruiz, E., & Hix, W. R. 2008, *ApJ*, 679, 1385
- . 2009, *ApJ*, 695, 404
- Sari, R., Piran, T., & Narayan, R. 1998, *Astrophys. J.*, 497, L17
- Schady, P., Krühler, T., Greiner, J., et al. 2015, *A&A*, 579, A126
- Shcherbakov, R. V., Pe'er, A., Reynolds, C. S., et al. 2013, *ApJ*, 769, 85
- Shen, R.-F., Nakar, E., & Piran, T. 2016, *Mon. Not. Roy. Astron. Soc.*, 459, 171
- Shiokawa, H., Krolik, J. H., Cheng, R. M., Piran, T., & Noble, S. C. 2015, *ApJ*, 804, 85
- Stratta, G., Gendre, B., Atteia, J. L., et al. 2013, *ApJ*, 779, 66
- Strubbe, L. E., & Quataert, E. 2009, *MNRAS*, 400, 2070
- Suwa, Y., & Ioka, K. 2011, *ApJ*, 726, 107
- Svirski, G., Piran, T., & Krolik, J. 2015, *ArXiv e-prints*, arXiv:1508.02389
- Thompson, C., & Duncan, R. C. 1993, *ApJ*, 408, 194
- . 1995, *MNRAS*, 275, 255
- Thompson, T. A., Chang, P., & Quataert, E. 2004, *ApJ*, 611, 380
- Thöne, C. C., de Ugarte Postigo, A., Fryer, C. L., et al. 2011, *Nature*, 480, 72
- Toma, K., Ioka, K., Sakamoto, T., & Nakamura, T. 2007, *ApJ*, 659, 1420
- Usov, V. V. 1992, *Nature*, 357, 472
- Waxman, E., Mészáros, P., & Campana, S. 2007, *ApJ*, 667, 351
- Wheeler, J. C., Yi, I., Höflich, P., & Wang, L. 2000, *ApJ*, 537, 810
- Woosley, S. E. 2010, *ApJ*, 719, L204
- Yan, L., Quimby, R., Ofek, E., et al. 2015, *ApJ*, 814, 108
- Zauderer, B. A., Berger, E., Soderberg, A. M., et al. 2011, *Nature*, 476, 425
- Zhang, B.-B., Zhang, B., Murase, K., Connaughton, V., & Briggs, M. S. 2014, *ApJ*, 787, 66